Original Article

JCBFM

Journal of Cerebral Blood Flow & Metabolism
2021, Vol. 41(3) 641–655

DOI: 10.1177/0271678X20926787
journals.sagepub.com/home/jcbfm
SAGE

MicroRNA-30a regulates acute cerebral ischemia-induced blood–brain barrier damage through ZnT4/zinc pathway

Peng Wang[1], Rong Pan[2], John Weaver[2], Mengjie Jia[1], Xue Yang[1], Tianhui Yang[1], Jia Liang[1] and Ke J Liu[2]

Abstract

The mechanism of early blood–brain barrier (BBB) disruption after stroke has been intensively studied but still not fully understood. Here, we report that microRNA-30a (miR-30a) could mediate BBB damage using both cellular and animal models of ischemic stroke. In the experiments in vitro, inhibition of miR-30a decreased BBB permeability, prevented the degradation of tight junction proteins, and reduced intracellular free zinc in endothelial cells. We found that the zinc transporter ZnT4 was a direct target of negative regulation by miR-30a, and ZnT4/zinc signaling pathway contributed significantly to miR-30a-mediated BBB damage. Consistent with these in vitro findings, treatment with miR-30a inhibitor reduced zinc accumulation, increased the expression of ZnT4, and prevented the loss of tight junction proteins in microvessels of ischemic animals. Furthermore, inhibition of miR-30a, even at 90 min post onset of middle cerebral artery occlusion, prevented BBB damage, reduced infarct volume, and ameliorated neurological deficits. Together, our findings provide novel insights into the mechanisms of cerebral ischemia-induced BBB disruption and indicate miR-30a as a regulator of BBB function that can be an effective therapeutic target for ischemic stroke.

Keywords

Blood–brain barrier, ischemic stroke, microRNA-30a, zinc, ZnT4

Received 21 November 2019; Revised 19 April 2020; Accepted 22 April 2020

Introduction

Blood–brain barrier (BBB) disruption at the early stage of ischemic stroke is a major cause of brain parenchymal injury[1] and regarded as a promising target for decreasing the hemorrhagic complications of thrombolytic therapy. The mechanism of early BBB disruption after stroke has been intensively investigated but still not fully understood. MicroRNAs (miRNAs) are small, noncoding RNAs that influence target gene expression through mRNA degradation and translation inhibition. Although many studies have examined the role of miRNAs in the pathogenesis of stroke-induced brain injury, much less attention has been paid to the functional significance of miRNAs in the BBB disruption after stroke. Recent studies of miRNAs expression in the brain microvascular endothelium revealed a set of miRNAs modulating BBB function under inflammatory conditions.[2] It was reported that overexpression of brain endothelial miR-98 and Let-7g-3p prevented BBB dysfunction by targeting the inflammatory molecules, CCL2 and CCL5 in neuroinflammation.[3] Another miRNA therapeutic target for central nervous system neuroinflammatory disorder is brain endothelial miR-155, a negative regulator of BBB function.[4] To date, little is known

[1]Key Laboratory of Neurodegenerative Diseases of Liaoning Province, Jinzhou Medical University, Jinzhou, China
[2]Department of Pharmaceutical Sciences, University of New Mexico Health Sciences Center, Albuquerque, NM, USA

Corresponding authors:
Ke J Liu, Department of Pharmaceutical Sciences, University of New Mexico Health Sciences Center, Albuquerque, NM 87131, USA.
Email: kliu@salud.unm.edu
Jia Liang, Key Laboratory of Neurodegenerative Diseases of Liaoning Province, Jinzhou Medical University, Jinzhou 121001, Liaoning, China.
Email: liangjia@jzmu.edu.cn

about whether miRNAs play any significant role in the acute cerebral ischemia-induced BBB disruption.

MicroRNA-30a (miR-30a), a member of the miR-30 family, was abundant in human endothelial cells (ECs) and has been shown to regulate gene expression relevant to hypertension.[5,6] Researchers collected blood samples from 197 patients with ischemic stroke and they found circulating miR-30a might be useful biomarkers for ischemic stroke in humans.[7] Moreover, the miR-30a in cerebral cortex of middle cerebral artery occlusion (MCAO) mice could be inhibited by hypoxic preconditioning pretreatment.[8] Therefore, miR-30a might be involved in the development of the brain endogenous protective strategy. Our recent studies showed that miR-30a could regulate ischemia-induced cell death in primary cultured cortical neurons and mouse brain after ischemia.[9,10] However, whether miR-30a exerts any effect on BBB disruption after ischemic stroke is unclear.

We have reported that ischemia triggers zinc accumulation in the ischemic cerebral microvessels, which critically contributes to acute BBB disruption following ischemic stroke.[11] However, the mechanisms of intracellular zinc accumulation in the microvessels after ischemia are unknown. Under ischemic conditions, cells may have altered ability to uptake and accumulate zinc intracellularly. The zinc transporter (ZnT), ZnT4, located in the plasmatic membrane, mediates zinc efflux from cytoplasm to prevent an excessive rise of its intracellular concentration.[12] MiR-30a is highly conserved between human, mouse, and rat with perfect match in the 3′-untranslated region (UTR) of ZnT4 mRNA in these species, suggesting that miR-30a could target and regulate ZnT4. Therefore, we hypothesize that miR-30a may play an important role in zinc-mediated BBB disruption via ZnT4 following acute cerebral ischemia.

In this study, using in vitro and in vivo ischemic BBB models, we examined the role of miR-30a in acute BBB disruption, and explored the possible mechanisms of miR-30a-mediated BBB permeability during the acute cerebral ischemia.

Materials and methods

Cell culture

Brain microvascular EC bEnd3, pericyte cell line MBVP, astrocytic cell C8-D1A, and Dulbecco's modified Eagle medium (DMEM) were obtained from American Type Culture Collection (Manassas, VA, USA). Briefly, cells were cultured in DMEM supplemented with 10% fetal bovine serum (FBS), 100 U/mL penicillin, and 100 μg/mL streptomycin (Life Technologies, CA, USA) at 37 °C in 5%CO_2/95% air.

Construction of in vitro BBB model

The in vitro BBB model was constructed according to the protocol described before.[13] Briefly, pericyte cell line MBVP were seeded on the bottom side of the collagen-coated polyester membrane of the inserts (Millipore, MA, USA). The cells were let to adhere to the membrane surface for 2 h, then bEnd3 cells were seeded on luminal side of the inserts placed in the well of the 24-well culture plates containing astrocytic cell C8-D1A.

Transfection of miR-30a mimic and inhibitor

To up- and down-regulate the expression of miR-30a in ECs, cells were seeded on plates at a density of 60–70% and transfected with miR-30a mimic, miR-30a inhibitor, or their controls (Exiqon A/S, Vedbaek, Denmark; GenePharma, Shanghai, China) at a final concentration of 25 nM according to manufacturer's instruction. The mimic control and inhibitor control were scrambled sequences. Cells were prepared for follow-up treatment and tested 48 h after transfection.

OGD treatment

To mimic ischemic-like condition in vitro, the ECs or co-cultured cells were exposed to oxygen and glucose deprivation (OGD), as we described previously.[14] Glucose-free DMEM was pre-equilibrated with 95% N_2/5% CO_2. ECs or co-cultured cells were incubated in a humidified airtight chamber (Billups-Rothberg Inc., Del Mar, CA, USA) equipped with an air lock and flushed with 95% N_2/5% CO_2 for 15 min. The chamber was sealed and kept at 37°C for 2 h, 4 h, or 6 h. The oxygen concentration was below 0.2% as monitored by an oxygen analyzer (Sable Systems, North Las Vegas, NV, USA). Control groups were incubated with DMEM without FBS at 37°C in 5% CO_2/95% air. Our previous study showed that zinc accumulates to high concentrations in microvessels in the first few hours of stroke. To mimic the ischemia-mediated increase of extracellular zinc, zinc chloride (100 μmol/L) was added to the media. The concentrations were selected based on our previous report.[11]

In vitro permeability assay

Permeability of the in vitro BBB model was measured as described previously.[14] In brief, after OGD treatment, 750 μL assay medium was added to each lower chamber and 150 μL assay medium containing 100 μg/mL fluorescein isothiocyanate labelled bovine serum albumin (FITC-BSA; Invitrogen, Carlsbad, CA) was added to each insert (upper chamber). Incubation continued for 1 h at 37°C in 5% CO_2/95% air. After the insert was removed, the medium in each lower chamber

was thoroughly mixed. Aliquots of 150 μL conditioned media were collected from the lower chamber. FITC-BSA assay medium and the assay medium itself (background) were used for measuring fluorescence intensity with a fluorescence plate reader. Permeability of the in vitro BBB model was quantified as clearance of FITC-BSA from the upper chamber to the lower chamber after subtracting background fluorescence intensity by using the equation: Clearance (%) = (Fluorescence in lower chamber/Total fluorescence added in upper chamber) × 100.

Transendothelial electrical resistance assay

Transendothelial electrical resistance (TEER) was measured by RE1600 voltohmmeter (Beijing Kingtech Technology Co. Ltd., China) according to the manufacturer's instruction. TEER values were calculated based on the formula: TEER ($\Omega \times cm^2$) = [TEER total (Ω) – TEER blank (Ω)] × 0.33 (cm^2).

Measurement of cell viability

The cell viability was evaluated by using thiazolyl blue tetrazolium bromide (0.5 mg/mL; Applichem Inc., Omaha, NE, USA) following the manufacturer's instruction.

Dual luciferase reporter assay

Each fragment of the 3′-UTR and mutant 3′-UTR of ZnT4 was amplified and cloned into the pmiR-RB-ReportTM luciferase reporter vector (RiboBio, Guangzhou, China). For the luciferase reporter assay, bEnd3 cells were co-transfected with pmiR-RB-ReportTM luciferase reporter vector, including the 3′-UTR of ZnT4 (either wild type or mutant), and miR-30a mimic or miR-30a control by using Lipofectamine 3000. Luciferase assays were performed by using the dual-luciferase reporter assay system (Promega, WI, USA) 48 h after transfection.

ZnT4 knockdown by small interfering RNA

Transfection of ZnT4 small interfering RNA (siRNA) (CGAUGACUCCUUAUUGGACTT) and a non-targeting vector as negative control (Life Technologies, CA, USA) was performed according to the protocol provided by Life Technologies.

Immunocytochemistry

The bEnd3 cells grown on glass coverslips in 24-well culture plates were fixed with 4% paraformaldehyde followed by blocking with 3% bovine serum albumin-phosphate buffered saline (PBS) for 1 h at room temperature. The cells were then incubated overnight at 4°C with the following primary antibodies: anti-claudin-5 (1:50, Invitrogen, CA, USA), anti-occludin (1:50, Invitrogen), and anti-ZnT4 (1:100, Absin, Shanghai, China). After washing, cells were incubated with secondary antibodies conjugated with Alexa Fluor 488 (1:500, Invitrogen). Cells were then counterstained with 4′,6-diamidino-2-phenylindole (DAPI) for nuclear labeling. The coverslips were mounted on glass slides after washing in PBS. Fluorescence images were captured with a fluorescence microscope (DMI4000B; Leica Microsystems, Wetzlar, Germany).

Animal model of focal cerebral ischemia/reperfusion

All animal experimental procedures in this study were approved by the Institutional Animal Care and Use Committee of University of New Mexico (NM, USA), in concordance with the National Institutes of Health guidelines for care and use of laboratory animals and the Animals in Research: Reporting In Vivo Experiments guidelines. Animals were housed under standard laboratory conditions. Food and water were available ad libitum. Male Sprague-Dawley rats (290–320 g, 9–12 weeks old) were anesthetized with 2% isoflurane in N_2O:O_2 (70%:30%) and subjected to focal cerebral ischemia using the suture occlusion model, as we previously described.[15] The rats underwent 2 h MCAO and then were reperfused for 72 h by withdrawal of the monofilament suture. Rectal temperature was regularly maintained at 37.0°C during surgery with a homeothermic heating pad. The rats displayed typical neurologic deficit of MCAO, circling to the non-ischemic side, were included in this study. All outcome measures were performed by investigators blind to the experimental group.

Tail vein injection

Considering the possible applications in clinic, injection was performed at 90 min post MCAO onset, instead of pretreatment before ischemia to simulate a potential intervention in stroke patients. MiR-30a inhibitor or inhibitor scramble was injected via the lateral tail vein in a randomized way; the dose was 10 mg/kg in PBS, total injected volume was 300 μL. Dosage was recommended by the instruction manual. Inhibitor scramble was used as a negative control.

Evaluation of BBB permeability in ischemic rats by Evan's Blue leakage

Evan's Blue (EB, 2% wt/vol in PBS; Sigma) was intravenously administered via tail vein after 2 h MCAO/70 h reperfusion. After 2 h circulation (at the end of 72 h reperfusion), the rats were transcardially perfused with saline. The brain was then removed and cut into

five 2-mm-thick coronal slices. Brain slices were photographed to visualize EB leakage. Quantitative assessment of BBB disruption was achieved by measuring EB content in the ischemic hemispheric tissue as we previously reported.[16] In brief, non-ischemic and ischemic hemispheric tissues were weighed and homogenized in 50% wt/vol trichloroacetic acid. The fluorescence intensity of the supernatant was measured on a microplate fluorescence reader. The EB content was calculated using a standard curve and expressed as ng per g of brain tissue.

Measurement of brain edema of ischemic rats

Measurement of brain edema is another way to assess the BBB damage after cerebral ischemia. In our study, brain edema was evaluated by measuring the hemispheric areas of each 2 mm thick brain slice on the digital photographs obtained as described previously.[17] Using ImageJ software, hemisphere enlargement was quantified as relative increase of the brain area in the ischemic hemisphere versus the non-ischemic hemisphere.

Measurements of neurological deficits and infarct volume

At the end of 72 h reperfusion, neurological deficits were assessed by a blinded investigator with two methods: Ludmila Belayev[18] and Zea-Longa score.[19]

After the evaluation of neurological deficits, brains were harvested and cut into 2-mm-thick coronal sections. The brain sections were incubated for 20 min in 0.5% 2,3,5-triphenyltetrazolium chloride (TTC; Sigma-Aldrich, St. Louis, MO, USA) solution at 37°C. The infarct area of each brain section was measured using the ImageJ Software.

Zinc detection by FluoZin-3

Intracellular zinc was measured by using FluoZin-3 (Invitrogen), a selective fluorescent probe for free zinc in cells. ECs were plated onto glass coverslips. After treatments, ECs were washed with DMEM three times to remove extracellular zinc before incubating with DMEM containing 2.5 μM FluoZin-3 for 45 min at room temperature. The coverslips were mounted on the glass slide after washing in DMEM. Images were acquired using a fluorescence microscope (Olympus OX71, Tokyo, Japan). Immunofluorescence intensity was quantified by ImageJ and all results were normalized to the cell number.

To visualize zinc accumulation in ischemic microvessels, we co-stained microvessels with FluoZin-3 and the endothelial marker Tomato Lectin. Briefly, at the end of reperfusion, Tomato Lectin (1.25 mg/kg; Vector Laboratories, CA, USA) was administrated by tail vein and circulated for 5 min to label the vessels. Then brains were harvested and cut into 20 μm slices. After incubation with 5 μmol/L FluoZin-3 for 1 h in the dark, the sections were counterstained with DAPI.

Immunohistochemical staining of occludin and claudin-5 in cerebral microvessels

To investigate the level of tight junction proteins (TJPs) in microvessels themselves after ischemia, we co-stained brain sections with the antibody of occludin or claudin-5 and the endothelial marker Tomato Lectin. Briefly, at the end of reperfusion, Tomato Lectin was administrated (see Section "Zinc detection by FluoZin-3" above). The primary antibodies were: occludin (1:500, Invitrogen), claudin-5 (1:500, Invitrogen), followed by secondary antibodies conjugated with Alexa Fluor 488 (1:1000, Invitrogen). The images of microvessels were captured using a fluorescence microscope after DAPI staining.

Isolation of cerebral microvessels from rat brain after ischemia/reperfusion

To examine the impacts of miR-30a on cerebral microvessels, we extracted cerebral microvessels from brains of ischemic rats as previously reported.[11] Briefly, at the end of 72 h reperfusion, the hemispheric cerebral tissue was minced and homogenized in ice-cold PBS. Then the homogenate was filtered through a 41 μm nylon mesh. Cerebral microvessels retained on the mesh were then purified with Dextran T-500 and stored at –80°C until further analysis.

Real-time RT-PCR

Total RNAs, including miRNAs from bEnd3 cells and isolated microvessels, were extracted with the miRCURY™ RNA Isolation Kit (Exiqon A/S, Vedbaek, Denmark) according to the manufacturer's protocol. Reverse transcription was performed by using the Universal cDNA synthesis kit II (Exiqon A/S, Vedbaek, Denmark). The quantitative real-time RT-PCR (qRT-PCR) amplification was performed with QuantStudio™ 3 Real-Time PCR Systems (Thermo Fisher Scientific, MA, USA) using ExiLENT SYBR® Green master mix (Exiqon A/S, Vedbaek, Denmark) according to the manufacturer's protocol, with U6 used as an internal control. Relative expression level was calculated with the following equation: relative gene expression $= 2^{-(\Delta Ct \text{ sample} - \Delta Ct \text{ control})}$.

Western blot analysis for occludin, claudin-5, and ZnTs in cultured ECs and isolated cerebral microvessels

Antibodies used in this study were anti-occludin polyclonal antibody (1:500, Invitrogen), anti-claudin-5 monoclonal antibody (1:1000; Invitrogen), anti-ZnT1 polyclonal antibody (1:1000, Absin, Shanghai, China), anti-ZnT2 polyclonal antibody (1:1000, Biorbyt, Cambridge, UK), anti-ZnT3 polyclonal antibody (1:1000, Proteintech, IL, USA), anti-ZnT4 polyclonal antibody (1:1000, Invitrogen), mouse anti-β-actin monoclonal antibody (1:1000; Santa Cruz Biotech.), and the IRDye 800CW goat anti-rabbit or IRDye 680RD goat anti-mouse as secondary antibodies (1:10,000, Li-cor). Cell lysate (30 µg of protein) was resolved on an SDS-PAGE (10% SDS gel) and transferred onto polyvinylidene difluoride membrane (Bio-Rad, Hercules, CA), and incubated for 1 h in Tris-buffered saline with Tween (TBST; 10 mM Tris, pH 8.0, 150 mM NaCl, and 0.1% Tween 20) containing 10% non-fat milk. The membrane was then incubated overnight at 4°C with primary antibodies and with secondary antibodies for 1 h. Bands on membranes were detected using the Odyssey Infrared Imaging System (LI-COR) with Molecular Imaging Software V4.0.

Data analysis

Statistical analyses were performed using SPSS 19.0. Data reported were presented as mean ± SD. Statistical analysis was performed using Student's *t*-test or Mann–Whitney *U* test to determine statistical differences between two groups where appropriate. One-way analysis of variance followed by Bonferroni/Dunn post hoc test was used for multiple comparisons. A value of $p < 0.05$ was considered statistically significant.

Results

Inhibiting miR-30a decreases OGD-induced endothelial barrier disruption

To determine the expression of miR-30a in ECs after OGD, we examined miR-30a levels using qRT-PCR. Our results showed that miR-30a levels significantly increased at 2, 4, and 6 h after OGD (Figure 1(a)). To determine the effect of miR-30a on ischemia-induced BBB damage, we first used miR-30a mimic or miR-30a inhibitor to up- or down-regulate miR-30a in the BBB model in vitro. MiR-30a level was significantly increased by transfection with miR-30a mimic and dramatically decreased by transfection with miR-30a inhibitor (Figure 1(b) and (e)). The results of FITC-BSA permeability and TEER value demonstrated that exposure of the triple cell co-culture model to 2–6 h OGD induced marked alterations in BBB integrity. MiR-30a mimic could increase OGD-induced FITC-BSA permeability and reduce the TEER value, whereas miR-30a inhibitor could effectively inhibit OGD-induced FITC-BSA permeability and increase the TEER value (Figure 1(c), (d), (f), and (g); Supplementary Figure 1). Meanwhile, we also found that OGD-induced reduction of EC viability was recovered by treatment with miR-30a inhibitor (Figure 1(h)).

Altered distribution of TJPs, particularly occludin and claudin-5, or their loss from microvessels is frequently seen in the compromised BBB following cerebral ischemia and reperfusion.[16,17] We examined whether the altered BBB permeability by miR-30a was due to the loss of TJPs under OGD condition. The changes of occludin and claudin-5 in ECs from inhibitor scramble, and miR-30a inhibitor groups are shown in Figure 1(i) and (l). Statistical analysis indicates that the loss of occludin and claudin-5 in control (inhibitor scramble) groups progressively deteriorated with increased duration of OGD treatment. Meanwhile, miR-30a inhibitor markedly blocked the loss of occludin and claudin-5 comparing with the inhibitor scramble groups (Figure 1(j) and (k)).

These findings indicate that inhibiting miR-30a could decrease the permeability and block the loss of TJPs in OGD-treated in vitro BBB model.

MiR-30a regulates the intracellular level of free zinc in brain microvascular ECs under OGD condition

The results above clearly show that inhibition of miR-30a could reduce OGD-induced endothelial barrier disruption. We then investigated the mechanism by which miR-30a mediated the OGD-induced endothelial barrier disruption in vitro. Our previous study reported zinc accumulation in ischemic microvessels leads to BBB disruption after ischemia.[11] Therefore, we sought to determine whether miR-30a regulates intracellular free zinc under OGD condition in vitro. MiR-30a mimic or inhibitor was used to treat bEnd.3 cells, and cells were treated with 100 µM zinc under 2 h OGD condition that mimics the environment of ischemic brain. Intracellular free zinc was detected using FluoZin-3 fluorescence probe (Figure 2(a)). We found that under normoxia with or without zinc administration, low level of free zinc in bEnd.3 cells was detectable, while adding 100 µM extracellular zinc significantly increased intracellular free zinc under OGD condition, which is consistent with our previous reports.[20] MiR-30a mimic could significantly enhance the intracellular level of free zinc, whereas

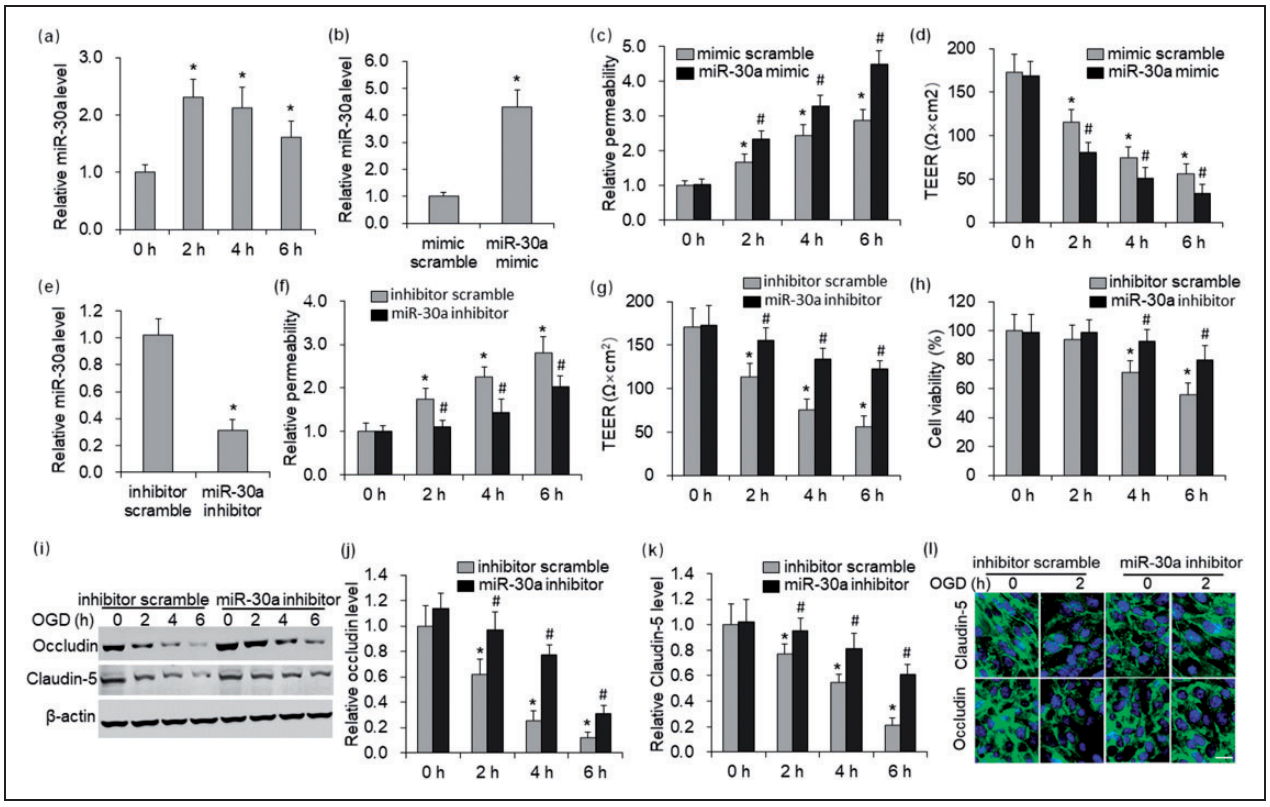

Figure 1. Effects of miR-30a on the barrier function and cell viability in BBB model in vitro. Mimic scramble and inhibitor scramble were used as negative controls. (a) Expression of miR-30a was determined by qRT-PCR in bEnd.3 cells exposed to 0 h, 2 h, 4 h, 6 h OGD. $^{*}P < 0.05$ vs. 0 h, $n = 4$/group. (b) and (e) Expression of miR-30a was determined by qRT-PCR in bEnd.3 cells transfected with miR-30a mimic, miR-30a inhibitor or their controls. $^{*}P < 0.05$ vs. mimic scramble or inhibitor scramble, $n = 4$/group. (c) and (f) After the triple cell co-culture model was treated with miR-30a mimic, miR-30a inhibitor, or their controls, the integrity of the endothelial barrier was evaluated by quantifying the FITC-BSA permeability. (d) and (g) TEER was evaluated after miR-30a mimic or miR-30a inhibitor treatment. (h) EC viability was evaluated after miR-30a inhibitor treatment. (i) The levels of occludin and claudin-5 in bEnd.3 cells were evaluated by using Western blot. (j) Quantitative analysis of occludin level. (k) Quantitative analysis of claudin-5 level. (l) Immunofluorescent staining for claudin-5 (green)/DAPI (blue) and occludin (green)/DAPI (blue). Scale bar: 20 μm. $^{*}P < 0.05$ vs. 0 h mimic scramble or inhibitor scramble group, $^{\#}P < 0.05$ vs. mimic scramble or inhibitor scramble at the same time after OGD, $n = 4$/group.
miR-30a: microRNA-30a; TEER: transendothelial electrical resistance; OGD: oxygen and glucose deprivation.

miR-30a inhibitor decreased the intracellular level of free zinc (Figure 2(b)). These results demonstrate that miR-30a could regulate intracellular level of free zinc under OGD condition.

To demonstrate the contribution of miR-30a to the biological effects of zinc on brain endothelial barrier integrity, we transfected miR-30a inhibitor in zinc-treated ECs, and then measured the permeability and TEER in the triple cell co-culture model (Figure 2(c) and (d); Supplementary Figure 2), occludin, and claudin-5 levels (Figure 2(e) to (g)) in ECs after 2 h OGD. The results show that adding zinc greatly increased FITC-BSA permeability, reduced the TEER value, and exacerbated the loss of TJPs under OGD condition. Most importantly, inhibition of miR-30a largely abolished zinc-induced effects on 2 h OGD-treated ECs. These results suggest that miR-30a plays an important role in zinc-mediated BBB disruption.

ZnT4 is a direct target of miR-30a

To explore the possible mechanism of miR-30a inhibitor in decreasing intracellular zinc accumulation, we performed bioinformatics analysis by TargetScan7.2 search and found a binding site for miR-30a at the 3′-UTR of ZnT4 mRNA with a high possibility ranking (Figure 3(a), aggregate probability of conserved targeting (PCT) score 0.95, rank 164/1576), implying that miR-30a may repress translation of ZnT4. Dual-luciferase assay verified that miR-30a mimic significantly inhibited luciferase activity of the reporter

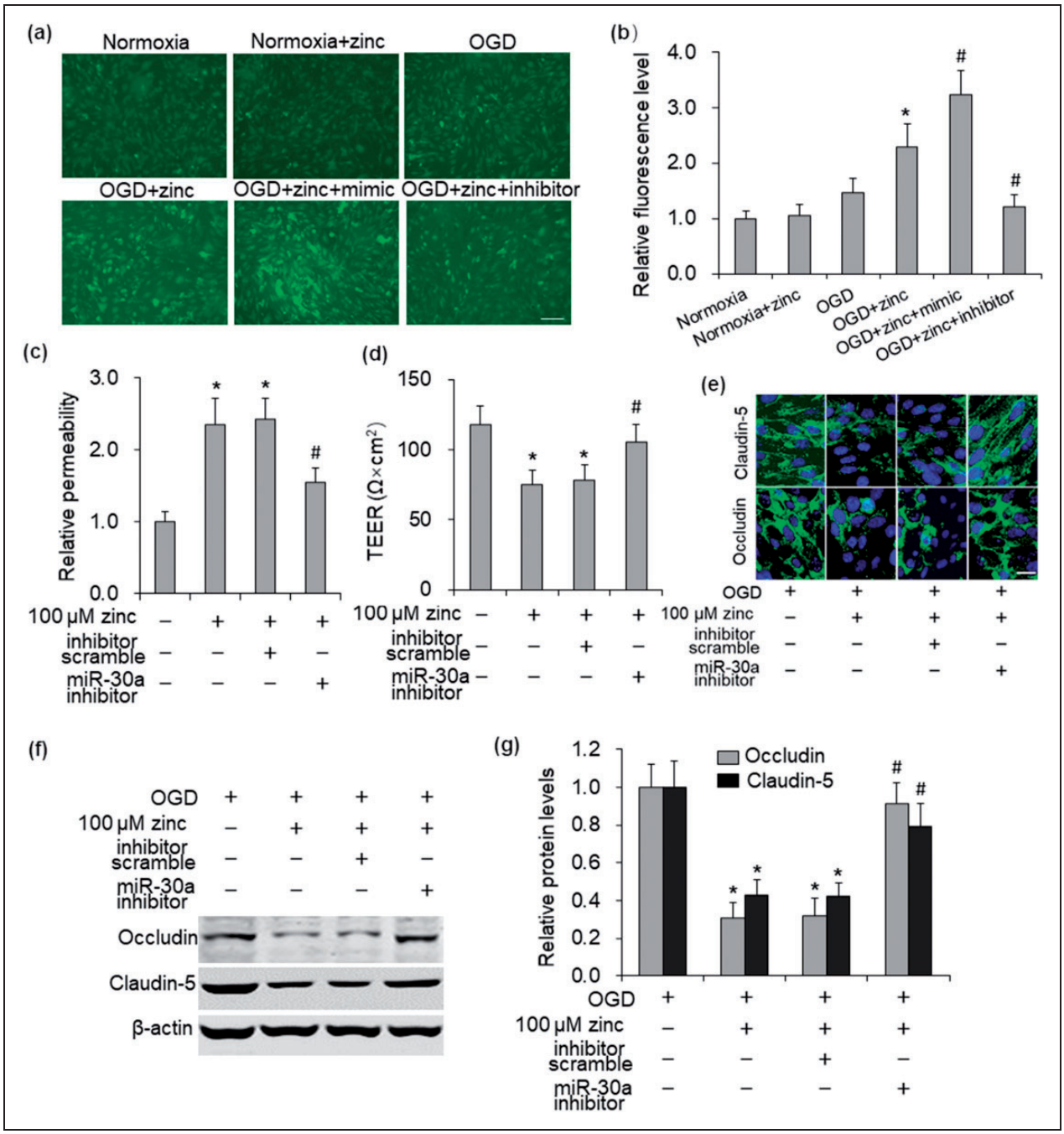

Figure 2. Effect of miR-30a on intracellular zinc under OGD condition. (a) The intracellular free zinc was visualized using FluoZin-3 fluorescence probe under various treatment conditions. Scale bar: 50 μm. (b) Quantitative analysis of fluorescence level. (c) and (d) The integrity of the endothelial barrier was evaluated by quantifying the FITC-BSA permeability and TEER after 2 h OGD. (e) Immunofluorescent staining for claudin-5 (green)/DAPI (blue) and occludin (green)/DAPI (blue). Scale bar: 20 μm. (f) The levels of occludin and claudin-5 in bEnd.3 cells were measured by using Western blot. β-actin was used as a loading control. (g) Quantitative analysis of occludin and claudin-5 levels. $^{*}P < 0.05$ vs. OGD; $^{\#}P < 0.05$ vs. OGD + zinc. $n = 4$/group.
OGD: oxygen and glucose deprivation; miR-30a: microRNA-30a.

vector containing the intact miR-30a binding site but not the mutant 3′-UTR of ZnT4 (Figure 3(b)). These results identified ZnT4, one of zinc transporter proteins, as a potential target for miR-30a interaction.

To test experimentally whether ZnT4 is regulated by miR-30a, bEnd.3 cells were transfected with miR-30a mimic or miR-30a inhibitor. As shown in Figure 3(c) to (h), up-regulation of miR-30a with miR-30a mimic

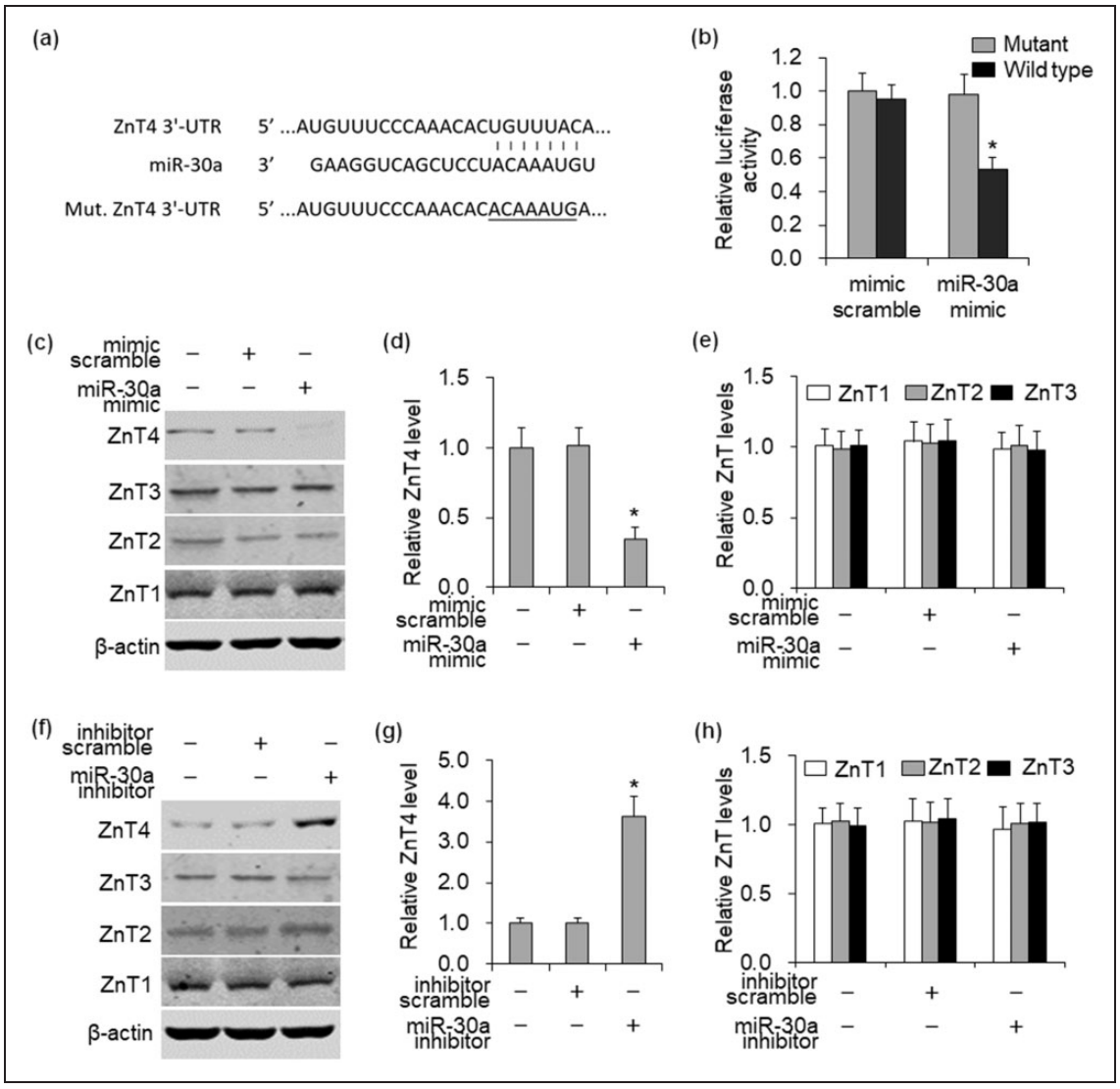

Figure 3. ZnT4 is a direct target of miR-30a. (a) Specific binding sequence of miR-30a on ZnT4 mRNA and mutant sequence integrated in dual-luciferase reporter plasmid were presented. (b) Luciferase reporter assay was performed by co-transfection of luciferase reporter containing 3′-UTR (wild type or mutant) of ZnT4 with miR-30a mimic or mimic scramble into bEnd.3 cells. (c) and (f) The levels of ZnTs in bEnd.3 cells were measured using Western blot. β-actin was used as a loading control. (d) and (g) Quantitative analysis of ZnT4 levels. (e) and (h) Quantitative analysis of ZnT1-3 levels. $^*P < 0.05$ vs. mimic scramble or inhibitor scramble. $n = 4$/group.
miR-30a: microRNA-30a.

down-regulated ZnT4, whereas down-regulation of miR-30a with miR-30a inhibitor greatly up-regulated ZnT4. There were no significant differences in the ZnT1, ZnT2, and ZnT3 protein levels. These results suggest that miR-30a could directly recognize the 3′-UTR of ZnT4 mRNA to negatively regulate ZnT4 protein level.

Inhibition of miR-30a decreases ischemia-induced BBB disruption through ZnT4/zinc pathway

To determine whether ZnT4 regulates the intracellular level of free zinc, we used siRNA to silence the expression of ZnT4 in bEnd.3 cells treated with 100 μM zinc under 2 h OGD condition mimicking the environment of ischemic brain. Immunofluorescent staining and Western blot analysis showed that ZnT4 siRNA effectively knocked down ZnT4 protein level in bEnd.3 cells at 48 h after ZnT4 siRNA transfection (Figure 4(a) to (c)). Knocking down ZnT4 resulted in a significantly increase of the intracellular level of free zinc (Figure 4(d) and (e)). These results demonstrate that ZnT4 plays an important role in regulating intracellular level of free zinc.

To confirm whether miR-30a exerts its effect on brain endothelial barrier integrity through regulation

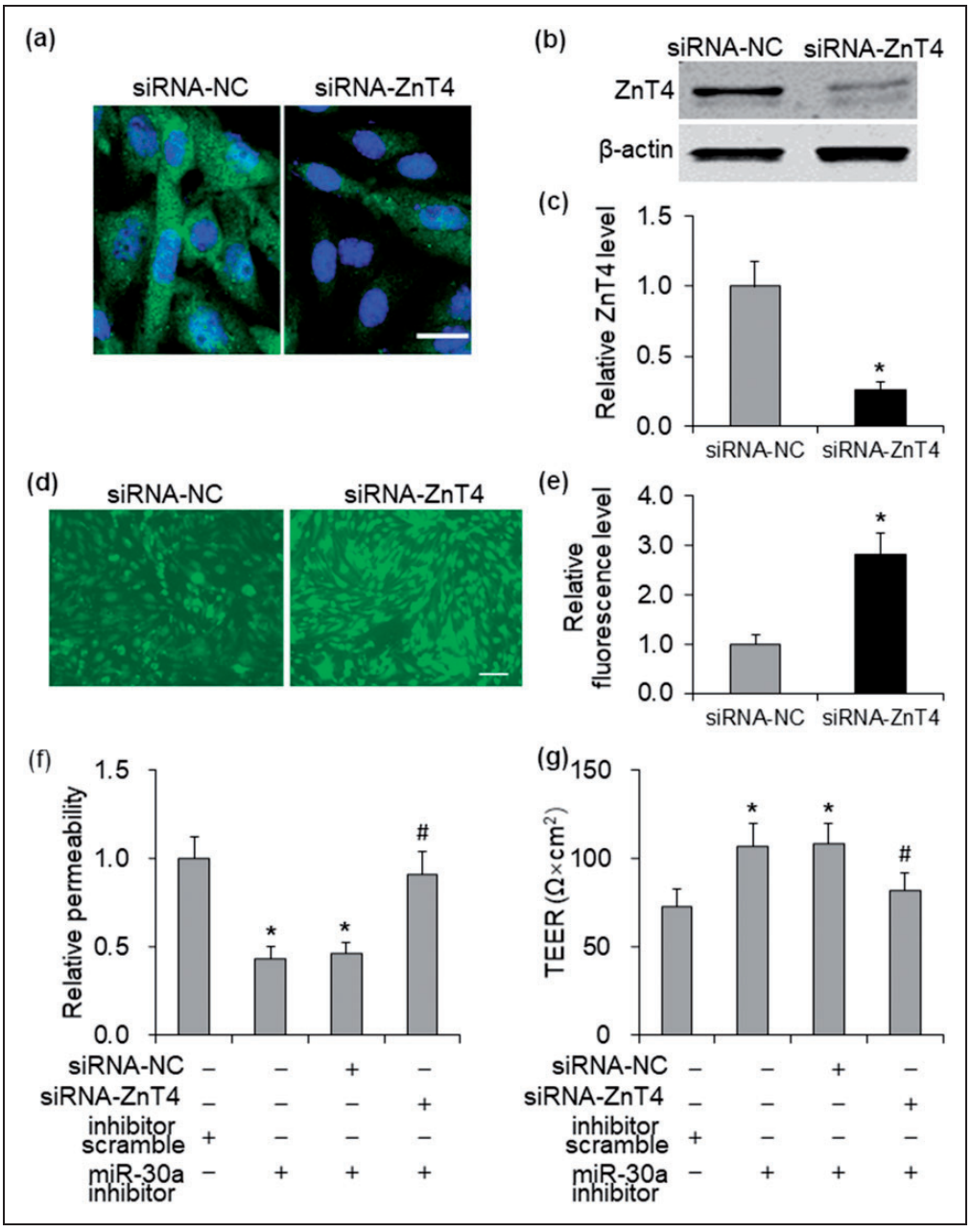

Figure 4. ZnT4 plays an important role in intracellular zinc regulation and miR-30a-mediated endothelial barrier integrity. (a) Co-staining of ZnT4 (green) and DAPI (blue). Scale bar: 20 μm. (b) Representative immunoblots of ZnT4 and the loading control β-actin. (c) Quantitative data of ZnT4 level. Representative image (d) and quantitative analysis (e) of zinc fluorescence after 2 h OGD treatment. Scale bar: 50 μm. $^{*}P < 0.05$ vs. siRNA-NC, $n = 4$/group. (f) and (g) The barrier integrity of the triple cell co-culture model increased after miR-30a inhibition, and this effect of miR-30a inhibitor was reversed by ZnT4 siRNA. $^{*}P < 0.05$ vs. inhibitor scramble. $^{\#}P < 0.05$ vs. miR-30a inhibitor. $n = 4$/group.
siRNA-NC: siRNA-ZnT4 negative control group; miR-30a: microRNA-30a.

of ZnT4, we measured the BBB permeability and TEER in the triple cell co-culture model after co-transfection miR-30a inhibitor and ZnT4 siRNA. Our results show that inhibition of ZnT4 expression by using siRNA blocked the miR-30a inhibitor-induced protective effect on brain endothelial barrier integrity under condition of 2 h OGD with exogenously added zinc (Figure 4(f) and (g); Supplementary Figure 3). Together, these results from in vitro experiments demonstrate inhibition of miR-30a decreases ischemia-induced BBB disruption by reducing intracellular levels of free zinc via ZnT4.

MiR-30a inhibitor reduced zinc accumulation and rescued the loss of ZnT4 in the microvessels of ischemic brain

To examine whether zinc accumulated in ischemic microvessels, brain slices were co-stained with zinc-specific fluorescence indicator (FluoZin-3), endothelium cell marker (Tomato Lectin), and nuclear-specific marker (DAPI). Zinc signal was almost invisible in Tomato Lectin-positive microvessels in non-ischemic hemisphere, whereas zinc fluorescence exhibited markedly increased and well co-localized with Tomato Lectin-labeled microvessels in ischemic hemisphere, indicating that ischemia/reperfusion lead to zinc accumulation in ischemic microvessels. Furthermore, administration of miR-30a inhibitor essentially prevented the zinc accumulation in ischemic microvessels (Figure 5(a)). These findings indicate that miR-30a

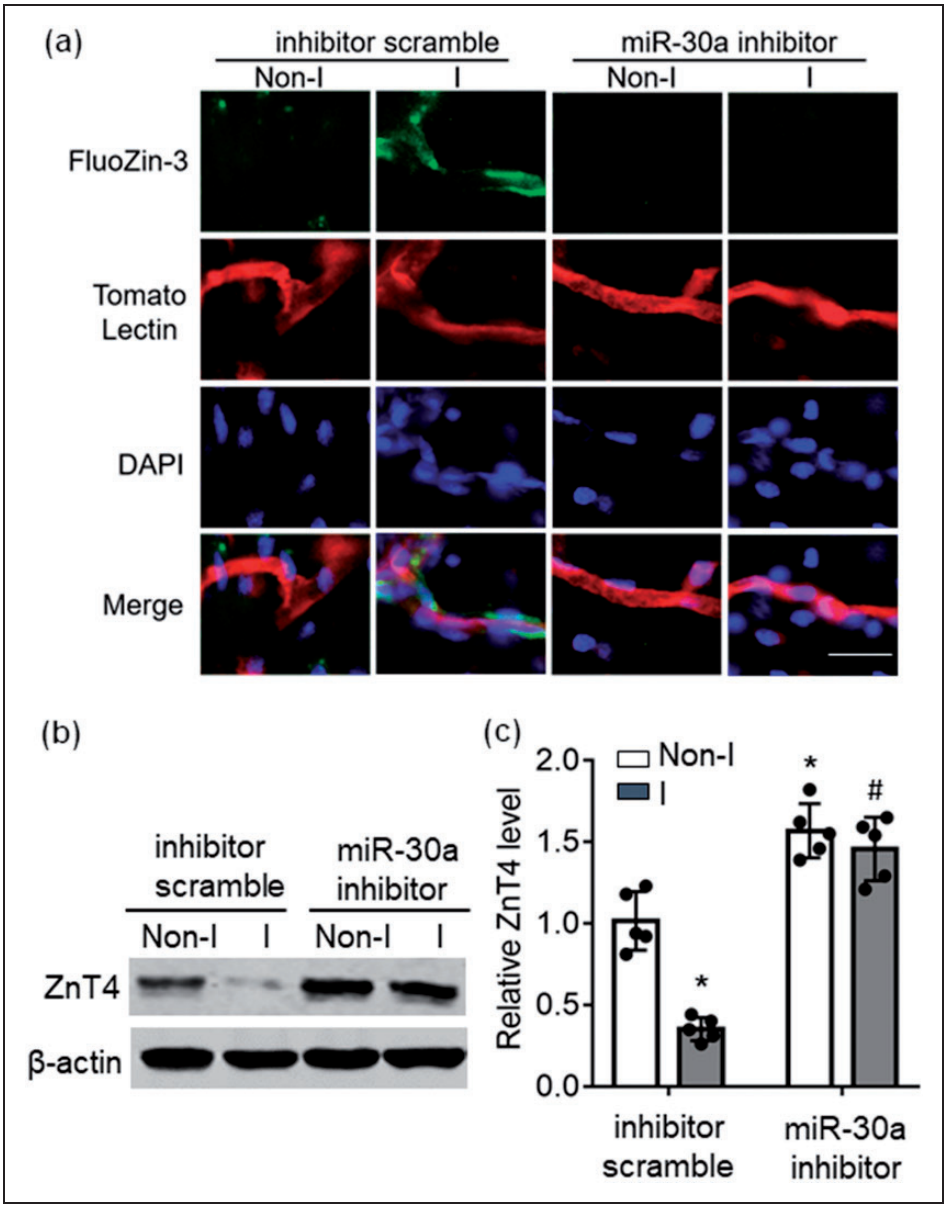

Figure 5. Effects of miR-30a on zinc accumulation and ZnT4 after cerebral ischemia in vivo. (a) Zinc accumulation in microvessels of brain slices was measured by co-staining of zinc-specific fluorescence indicator, FluoZin-3 (green) with Tomato Lectin (red) and nuclear marker (DAPI, blue). Scale bar: 20 μm. (b) The levels of ZnT4 were measured using Western blot in the extracts of microvessels isolated from ischemic rat brain. The level of β-actin was used as a loading control. (c) Quantitative analysis of ZnT4 level. $^{*}P < 0.05$ vs. contralateral hemisphere (Non-I) in inhibitor scramble group; $^{\#}P < 0.05$ vs. ischemic hemisphere (I) in inhibitor scramble group. $n = 5$/group.
miR-30a: microRNA-30a; DAPI: 4′,6-diamidino-2-phenylindole.

inhibitor decreased zinc accumulation in the microvessels in the ischemic region.

We also assessed the levels of ZnT4 in microvessels isolated from ischemic brain using Western blot (Figure 5(b)). It was shown that ZnT4 decreased in ischemic microvessels, while miR-30a inhibitor up-regulated ZnT4 in ischemic microvessels (Figure 5(c)). These results indicate that miR-30a regulates ZnT4 in microvessels isolated from ischemic rat brain.

MiR-30a inhibitor restored the loss of occludin and claudin-5 in microvessels of ischemic stroke rats

We further investigated whether the expression of TJPs could be influenced by miR-30a inhibitor in microvessels of ischemic stroke rats. We measured the levels of occludin and claudin-5 in microvessels by using immunohistochemistry approach. The fluorescence intensity of occludin was high in non-ischemic microvessels, whereas ischemia/reperfusion markedly reduced occludin signal intensity in microvessels. Most importantly, treatment of miR-30a inhibitor in the ischemic animal rescued the loss of occludin in ischemic microvessels (Figure 6(a)). Similar results were observed in the fluorescence of claudin-5 in microvessels (Figure 6(b)).

We also assessed the levels of occludin and claudin-5 in isolated microvessels using Western blot (Figure 6(c)). It was shown that both occludin (Figure 6(d)) and claudin-5 (Figure 6(e)) in microvessels decreased after

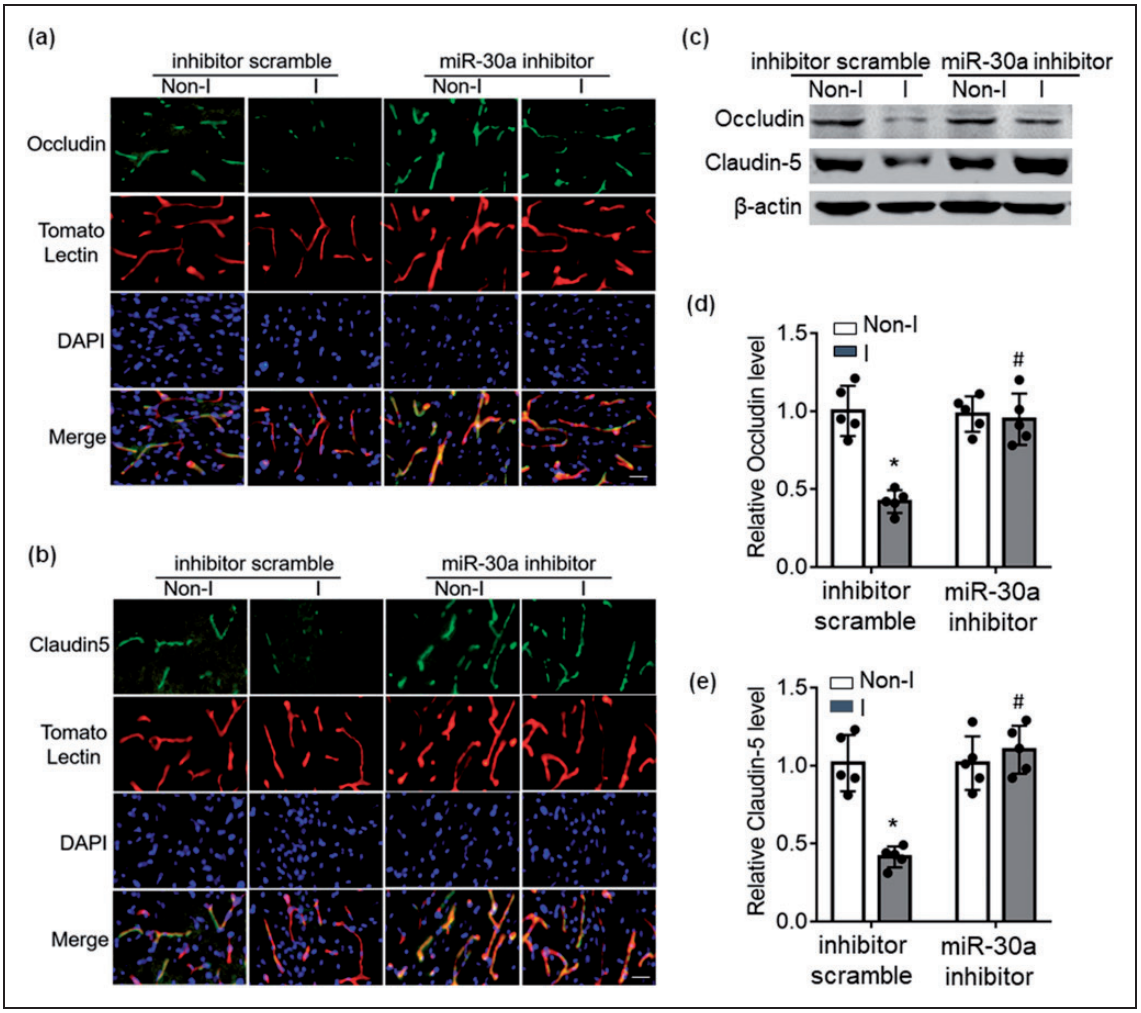

Figure 6. MiR-30a inhibitor prevents the loss of occludin and claudin-5 in microvessels isolated from ischemic rats. (a) Co-staining of occludin (green), Tomato Lectin (red), and DAPI (blue). (b) Co-staining of claudin-5 (green), Tomato Lectin (red), and DAPI (blue). Scale bar: 20 μm. (c) The representative bands of occludin and claudin-5 in microvessels isolated from ischemic rats using Western blot. (d) Quantitative analysis of occludin. (e) Quantitative analysis of claudin-5. $^{*}P < 0.05$ vs. contralateral hemisphere (Non-I) in inhibitor scramble group; $^{\#}P < 0.05$ vs. ischemic hemisphere (I) in inhibitor scramble group. $n = 5$/group.
miR-30a: microRNA-30a; DAPI: 4′,6-diamidino-2-phenylindole.

ischemia, while miR-30a inhibitor completely restored each of them to the non-ischemic control level. These results indicate that inhibition of cerebral miR-30a prevented ischemia-induced loss of TJPs in microvessels.

MiR-30a inhibitor decreases ischemia-induced BBB injury in vivo

We next examined the effect of miR-30a on BBB damage in vivo. FITC-conjugated miR-30a inhibitor or inhibitor scramble was administrated at 90 min post MCAO onset instead of pretreatment before ischemia. Fluorescence microscopy detected FITC-positive oligonucleotides (green, Supplementary Figure 4, arrows) associated with cerebral microvessels. Some fluorescein-labeled molecules also crossed the BBB and were seen in the brain parenchyma (Supplementary Figure 4, stars). Administration of miR-30a inhibitor severely decreased the level of miR-30a in cerebral microvessels from brain of ischemic rats (Figure 7(a)). EB extravasation and brain edema were used to assess the severity of BBB damage after ischemia/reperfusion. We found that cerebral ischemia/reperfusion significantly increased EB leakage in ischemic hemispheres, and miR-30a inhibitor markedly reduced EB extravasation in ischemic hemispheres (Figure 7(b) and (c)). Similarly, treatment with the miR-30a inhibitor significantly reduced ischemia-induced hemisphere edema (Figure 7(d)). These results indicate that inhibition of cerebral miR-30a provides neurovascular protection against disrupting BBB integrity following cerebral ischemia.

To determine whether miR-30a inhibitor provides sustained protection, we evaluated cerebral infarction and neurological functions at 72 h after reperfusion. Notably, miR-30a inhibitor reduced cerebral infarct volume relative to the inhibitor scramble group (Figure 7(e) and (f)). Similar protective effects of miR-30a inhibitor were observed for neurological function assessment using Ludmila Belayev (Figure 7(g)) and Zea-Longa scores (Figure 7(h)). It is worth noting that miR-30a inhibitor treatment did not affect cerebral blood flow (Supplementary Figure 5) and other physiological parameters (Supplementary Table 1) compared to control. Collectively, these in

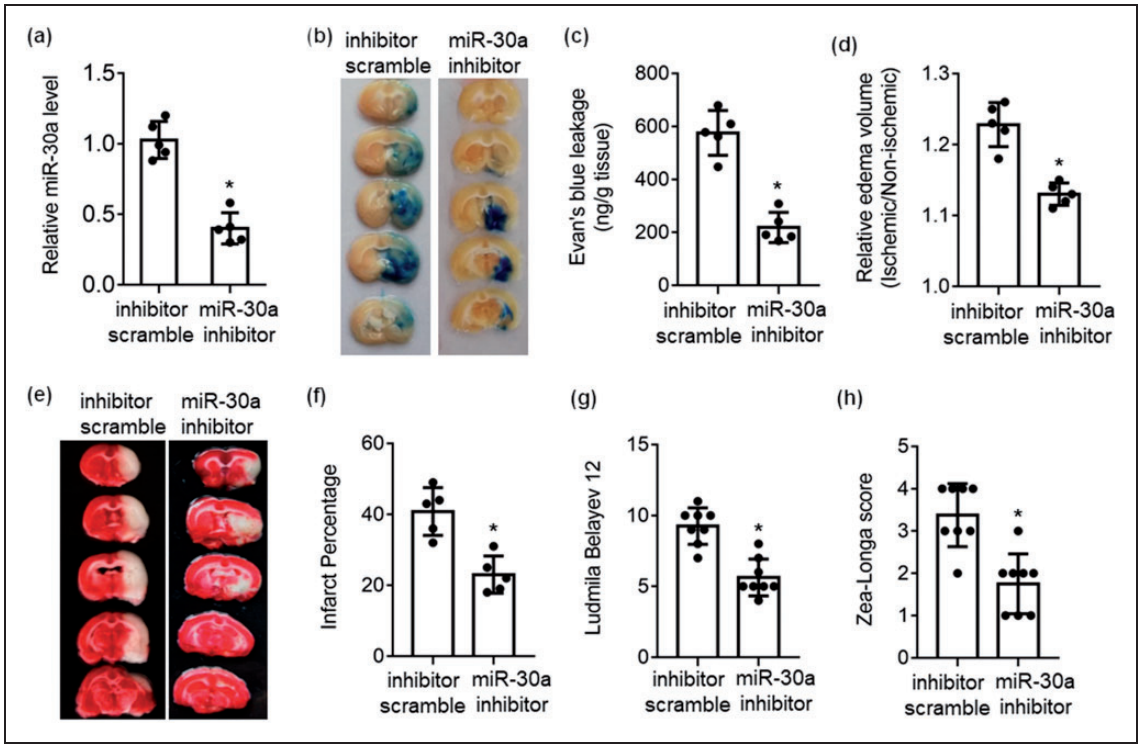

Figure 7. MiR-30a inhibitor reduces ischemia-induced BBB injury in vivo. (a) MiR-30a expression in the cerebral microvessels isolated from brain of ischemic rats injected with miR-30a inhibitor or scrambled control. (b) EB extravasation was measured to evaluate the BBB permeability after 2 h ischemia/72 h reperfusion. Brain slices showed EB extravasation (blue dye leakage) in inhibitor scramble and miR-30a inhibitor groups. (c) Quantitative analysis of EB content in ischemic hemisphere. (d) Quantitative analysis of relative edema volume by measuring ischemic hemispheric enlargement. (e) Representative TTC-stained coronal sections illustrating infarction in rats with 2 h MCAO plus 72 h reperfusion. (f) Quantitative analysis of infarction volume. (g) Ludmila Belayev neurological scores were assessed. (h) Zea-Longa neurological scores was evaluated. $^{*}P < 0.05$ vs. inhibitor scramble. $n = 5$–8/group.
miR-30a: microRNA-30a.

vivo findings strongly suggest that miR-30a inhibitor prevents BBB disruption and improves histological and neurological outcomes after ischemia.

Discussion

MiRNAs have emerged as key gene regulators in many diseases, including stroke. This is the first study to investigate the role of miR-30a in ischemia-induced BBB damage, in vitro and in vivo. Our results demonstrate that inhibition of miR-30a significantly decreased the neurovascular complications after cerebral ischemia. The mechanisms of miR-30a in BBB injury may involve regulating zinc concentration by targeting ZnT4. Findings from our experiments provide a novel insight into the role of miRNAs in BBB disruption during acute cerebral ischemia.

Recent studies have indicated the importance of miRNAs in the regulation of BBB function. MiR-155 inhibition at subacute phase of ischemia led to preservation of brain endothelial TJPs integrity and promoted recovery after experimental mouse stroke.[21] In addition, miR-150 inhibitor significantly ameliorated BBB disruption in permanent MCAO by directly targeting Tie-2, a factor involved in maintaining BBB integrity.[22] In ECs, members of the miR-30 family regulated vascular development and sprouting in angiogenesis.[23] A previous study revealed that miR-30a stimulated arteriolar branching by down-regulating the Notch ligand Dll4 expression, thereby controlling endothelial tip cell behavior.[5] The current study provides direct evidence that in vitro overexpression of miR-30a resulted in increased OGD-induced BBB permeability, whereas inhibition of miR-30a expression reduced OGD-induced BBB permeability.

TJPs between ECs are vital for the maintenance of BBB integrity, which restricts paracellular permeability.[24] The transmembrane proteins occludin and claudin-5 are key molecules sealing the gaps between adjacent ECs.[25] We investigated the role of miR-30a in the loss of occludin and claudin-5 proteins during cerebral ischemia. The results show that inhibition of miR-30a could rescue the loss of occludin and claudin-5 after ischemia, in vitro and in vivo.

The potential mechanisms of miR-30a-mediated BBB permeability after ischemia were explored in this study. We have reported that ischemia-induced zinc accumulation in the microvessels was a critical contributing factor to ischemia-induced BBB damage.[11] More interestingly, our results reveal that miR-30a could regulate intracellular level of free zinc under ischemia condition. Zinc has been reported to be released from neurons into extracellular space[26,27] and accumulate in microvessels thereby participate in BBB damage following ischemic stroke. But the mechanism of zinc accumulation in microvessels during cerebral ischemia is not well understood. Several studies have focused on zinc metabolism related to miRNAs.[28,29] In the present study, we found that exogenous zinc increased BBB permeability and exacerbated loss of TJPs in OGD-treated ECs. At the same time, inhibition of miR-30a reduced intracellular zinc accumulation and abolished zinc-induced effects. Our studies also provide the evidence that zinc accumulates in high concentration in ischemic microvessels. The involvement of miR-30a in zinc accumulation was further demonstrated in a rat model of ischemic stroke.

A major finding of the present study is that miR-30a could regulate the expression of ZnT4 both in vitro and in vivo. Dual-luciferase reporter assay also confirmed that ZnT4 is the direct target of miR-30a. Zinc homeostasis in cells is tightly regulated by two major protein groups. The Zrt/IRT-like protein family promotes zinc influx to cytoplasm and the ZnT family mediates zinc efflux from cytoplasm into intracellular compartments or out of the cells.[30,31] ZnT4 is involved in zinc homeostasis in the cerebral cortex after hypoxia–ischemia.[32] Our experimental results show that up-/down-regulation of miR-30a could enhance/decrease the intracellular level of free zinc through regulating the expression of ZnT4. A previous study from our lab demonstrates that down-regulated ZnT1 enhances zinc accumulation in astrocytes after ischemic stroke.[33] In the present study, we report that ZnT4 mediated intracellular zinc efflux in ECs and was involved in miR-30a-mediated BBB permeability, thus providing a novel mechanism for intracellular free zinc accumulation and BBB damage after ischemic stroke.

Very importantly, the present study shows inhibition of miR-30a protects BBB from ischemia-induced damage in a rat model of ischemic stroke. It is particularly worth noting that inhibition of miR-30a with miR-30a inhibitor, even at 90 min post MCAO onset, attenuated BBB impairment, as well as tissue damage, thereby offering functional improvements. EB extravasation and brain sampling were conducted at 72 h post ischemia since it is well recognized that the brain injury is stable or mature. Our findings suggest that miR-30a may be a novel target for reducing BBB damage at the early stage of cerebral ischemia, thus providing a clinically effective approach to diminish neurovascular complications from thrombectomy intervention and thrombolytic therapy.

In conclusion, our results demonstrate miR-30a could regulate acute ischemia-induced BBB permeability through ZnT4/zinc signaling pathway, and that inhibition of miR-30a could attenuate BBB breakdown and ischemic infarction, leading to better outcome. Our findings provide novel insights into the mechanisms of cerebral ischemia-induced BBB disruption and suggest

miR-30a is a negative regulator of BBB function that could be an effective therapeutic target for ischemic stroke.

Funding

The author(s) disclosed receipt of the following financial support for the research, authorship, and/or publication of this article: This work was supported by the National Natural Science Foundation of China (81971231); the China Scholarship Council (201608210006); the Scientific Research Project from the Educational Department of Liaoning Province (JYTQN201733); the Natural Science Foundation of Liaoning Province (201602319), and utilized the facility supported by the US National Institutes of Health (P30GM103400).

Declaration of conflicting interests

The author(s) declared no potential conflicts of interest with respect to the research, authorship, and/or publication of this article.

Authors' contributions

Peng Wang: conduct and analysis of the study and writing of the manuscript. Rong Pan, John Weaver, Mengjie Jia, Xue Yang, and Tianhui Yang: conduct of the study. Jia Liang: concept and design of the study and conduct of the study. Ke J Liu: concept and design of the study and review and editing of the manuscript.

Supplemental material

Supplemental material for this paper is available online.

References

1. Shi Y, Zhang L, Pu H, et al. Rapid endothelial cytoskeletal reorganization enables early blood–brain barrier disruption and long-term ischaemic reperfusion brain injury. *Nat Commun* 2016; 7: 10523.
2. Reijerkerk A, Lopez-Ramirez MA, Van Het Hof B, et al. MicroRNAs regulate human brain endothelial cell-barrier function in inflammation: implications for multiple sclerosis. *J Neurosci* 2013; 33: 6857–6863.
3. Rom S, Dykstra H, Zuluaga-Ramirez V, et al. miR-98 and let-7g* protect the blood-brain barrier under neuroinflammatory conditions. *J Cereb Blood Flow Metab* 2015; 35: 1957–1965.
4. Lopez-Ramirez MA, Wu D, Pryce G, et al. MicroRNA-155 negatively affects blood-brain barrier function during neuroinflammation. *FASEB J* 2014; 28, 2551–2565.
5. Jiang Q, Lagos-Quintana M, Liu D, et al. miR-30a regulates endothelial tip cell formation and arteriolar branching. *Hypertension* 2013; 62: 592–598.
6. Kriegel AJ, Baker MA, Liu Y, et al. Endogenous microRNAs in human microvascular endothelial cells regulate mRNAs encoded by hypertension-related genes. *Hypertension* 2015; 66: 793–799.
7. Long G, Wang F, Li H, et al. Circulating miR-30a, miR-126 and let-7b as biomarker for ischemic stroke in humans. *BMC Neurol* 2013; 13: 178.
8. Liu C, Peng Z, Zhang N, et al. Identification of differentially expressed microRNAs and their PKC-isoform specific gene network prediction during hypoxic pre-conditioning and focal cerebral ischemia of mice. *J Neurochem* 2012; 120: 830–841.
9. Wang P, Liang J, Li Y, et al. Down-regulation of miRNA-30a alleviates cerebral ischemic injury through enhancing beclin 1-mediated autophagy. *Neurochem Res* 2014; 39: 1279–1291.
10. Wang P, Zhang N, Liang J, et al. Micro-RNA-30a regulates ischemia-induced cell death by targeting heat shock protein HSPA5 in primary cultured cortical neurons and mouse brain after stroke. *J Neurosci Res* 2015; 93: 1756–1768.
11. Qi Z, Liang J, Pan R, et al. Zinc contributes to acute cerebral ischemia-induced blood-brain barrier disruption. *Neurobiol Dis* 2016; 95: 12–21.
12. Cousins RJ and McMahon RJ. Integrative aspects of zinc transporters. *J Nutr* 2000; 130: 1384S–1387S.
13. Lin HC, Ho MY, Tsen CM, et al. Comparative proteomics reveals silver nanoparticles alter fatty acid metabolism and amyloid beta clearance for neuronal apoptosis in a triple cell coculture model of the blood–brain barrier. *Toxicol Sci* 2017; 158: 151–163.
14. Li YN, Pan R, Qin XJ, et al. Ischemic neurons activate astrocytes to disrupt endothelial barrier via increasing VEGF expression. *J Neurochem* 2014; 129: 120–129.
15. Wang P, Lu Y, Han D, et al. Neuroprotection by nicotinamide mononucleotide adenylyltransferase 1 with involvement of autophagy in an aged rat model of transient cerebral ischemia and reperfusion. *Brain Res* 2019; 1723: 146391.
16. Liu W, Hendren J, Qin XJ, et al. Normobaric hyperoxia attenuates early blood-brain barrier disruption by inhibiting MMP-9-mediated occludin degradation in focal cerebral ischemia. *J Neurochem* 2009; 108: 811–820.
17. Liang J, Qi Z, Liu W, et al. Normobaric hyperoxia slows blood-brain barrier damage and expands the therapeutic time window for tissue-type plasminogen activator treatment in cerebral ischemia. *Stroke* 2015; 46: 1344–1351.
18. Belayev L, Alonso OF, Busto R, et al. Middle cerebral artery occlusion in the rat by intraluminal suture. Neurological and pathological evaluation of an improved model. *Stroke* 1996; 27: 1616–1622; discussion 1623.
19. Longa EZ, Weinstein PR, Carlson S, et al. Reversible middle cerebral artery occlusion without craniectomy in rats. *Stroke*. 1989; 20: 84–91.
20. Pan R, Chen C, Liu WL, et al. Zinc promotes the death of hypoxic astrocytes by upregulating hypoxia-induced hypoxia-inducible factor-1alpha expression via poly (ADP-ribose) polymerase-1. *CNS Neurosci Ther* 2013; 19: 511–520.
21. Caballero-Garrido E, Pena-Philippides JC, Lordkipanidze T, et al. *In vivo* inhibition of miR-155 promotes recovery after experimental mouse stroke. *J Neurosci* 2015; 35: 12446–12464.

22. Fang Z, He QW, Li Q, et al. MicroRNA-150 regulates blood-brain barrier permeability via Tie-2 after permanent middle cerebral artery occlusion in rats. *FASEB J* 2016; 30: 2097–2107.
23. Bridge G, Monteiro R, Henderson S, et al. The microRNA-30 family targets DLL4 to modulate endothelial cell behavior during angiogenesis. *Blood* 2012; 120: 5063–5072.
24. Wolburg H and Lippoldt A. Tight junctions of the blood-brain barrier: development, composition and regulation. *Vasc Pharmacol* 2002; 38: 323–337.
25. Liu J, Jin X, Liu KJ, et al. Matrix metalloproteinase-2-mediated occludin degradation and caveolin-1-mediated claudin-5 redistribution contribute to blood-brain barrier damage in early ischemic stroke stage. *J Neurosci* 2012; 32: 3044–3057.
26. Bitanihirwe BK and Cunningham MG. Zinc: the brain's dark horse. *Synapse* 2009; 63: 1029–1049.
27. Frederickson CJ, Giblin LJ, Krezel A, et al. Concentrations of extracellular free zinc (pZn)e in the central nervous system during simple anesthetization, ischemia and reperfusion. *Exp Neurol* 2006; 198: 285–293.
28. Grider A, Lewis RD, Laing EM, et al. Zinc affects miR-548n, SMAD4, SMAD5 expression in HepG2 hepatocyte and HEp-2 lung cell lines. *Biometals* 2015; 28: 959–966.
29. Ryu MS, Langkamp-Henken B, Chang SM, et al. Genomic analysis, cytokine expression, and microRNA profiling reveal biomarkers of human dietary zinc depletion and homeostasis. *Pro Natl Acad Sci USA* 2011; 108: 20970–20975.
30. Szewczyk B. Zinc homeostasis and neurodegenerative disorders. *Front Aging Neurosci* 2013; 5: 33.
31. Lichten LA and Cousins RJ. Mammalian zinc transporters: nutritional and physiologic regulation. *Annu Rev Nutr* 2009; 29: 153–176.
32. Aguilar-Alonso P, Martinez-Fong D, Pazos-Salazar NG, et al. The increase in zinc levels and upregulation of zinc transporters are mediated by nitric oxide in the cerebral cortex after transient ischemia in the rat. *Brain Res* 2008; 1200: 89–98.
33. Pan R and Liu KJ. ZNT-1 expression reduction enhances free zinc accumulation in astrocytes after ischemic stroke. *Acta Neurochir Supplement* 2016; 121: 257–261.